Dalton Transactions

ROYAL SOCIETY OF CHEMISTRY

COMMUNICATION

View Article Online
View Journal | View Issue

Check for updates

Cite this: *Dalton Trans.*, 2023, **52**, 15677

Received 20th September 2023,
Accepted 23rd October 2023

DOI: 10.1039/d3dt03080f

rsc.li/dalton

Photoinduced large magnetic change at room temperature and radical-quenched spin glass in a cyanide-bridged Mn^{II}–Fe^{III} compound†

Li-Zhen Cai, Xiao-Qing Yu, Ming-Sheng Wang * and Guo-Cong Guo *

By the coordination assembly of a redox photoactive functional motif and a cyanide-bridged moiety, a cyanide-bridged Mn^{II}–Fe^{III} compound with large photoinduced magnetic change at room-temperature due to photoinduced electron transfer was obtanied. This compound also shows unprecedented radical-quenched spin glass in molecule based magnets.

Photoresponsive magnetic materials, which change magnetism after the absorption of light,[1] have attracted intense interest in the past decades for their potential applications in memory and switches. Since the discovery of the first photomagnetic Prussian blue analog,[2] cyanide-bridged coordination compounds have become some of the most promising and most widely studied photomagnets.[3] They are usually obtained by photoswitching of spin numbers and/or exchange couplings based on various mechanisms,[4–6] such as metal-to-metal charge transfer (MMCT),[1,7–9] metal-to-ligand charge transfer (MLCT),[10–12] ligand-to-metal charge transfer (LMCT),[13–15] spin crossover of octahedrally coordinated d^4–d^7 transition metal,[16–20] isomerization of photochromic molecules,[21] and so on. Two critical problems have to be solved for the further development of such photomagnets. One is that the number of optional paramagnetic metals is very limited, although the selection of appropriate cyanide-bridged paramagnetic metals can produce the desired photomagnetism in the light of the well-known orbital-overlap principle.[22] The other is that most known examples change magnetism under illumination at cryogenic temperatures. Taking advantage of the light-excitation-in-the-thermal-hysteresis-loop technique, some cyanide-bridged coordination compounds display photomagnetism around room temperature (RT).[23,24] Even so, cyanide-bridged coordination compounds with thermal hysteresis loops around RT are rather rare. Therefore, obtaining room-temperature cyanide-bridged photomagnets remains a challenge.

Photochromic organic compounds usually change their molecular structures under illumination.[25] Incorporating them into spin systems as ligands or guest molecules/ions has been demonstrated to be an effective approach to modulating spin numbers and/or exchange couplings using light.[21,26–34] Their flexibilities of structural modification can enrich the cyanide-bridged photomagnetic systems, avoiding the limitation of optional paramagnetic metals. Their other important characteristic is that the photon mode commonly operates around RT. The presence of photochromic organic units in cyanide-bridged compounds very likely increases the photoswitching temperature for magnetism.

The most commonly used photochromic organic units in known photomagnetic compounds are those undergoing photo-induced *cis–trans* isomerization[21,26,27] or pericyclic reactions.[28–30,33,34] They require an adequate "breathing" space to allow photochromic reactions to occur due to their large structural change, otherwise the reactions would be prohibited or corruption of the crystal structure would occur.[6,32] In contrast, only minor structural distortion occurs after photocoloration for most electron-transfer (redox) photochromic organic species.[35–37] They generally generate radicals upon irradiation. It has been reported that radicals can antiferromagnetically or ferromagnetically couple with paramagnetic metals.[38,39] If redox photochromic organic units were incorporated into paramagnetic metal complexes as ligands, the resulting compounds could display photomagnetism at RT in the solid state.[40] To our knowledge, the photomagnetic effects of cyanide-bridged coordination compounds with redox photochromic organic units as ligands or guest ions have not been reported yet.

Previously, we reported that several photochromic halozinc coordination compounds of *N*-methyl-4,4′-bipyridinium cation (MQ^+) exhibit photoinduced halo atom to MQ^+ electron transfer with the formation of $MQ^{\bullet}$ radicals at RT.[41] Inspired by this, by introducing the redox photoactive MQ^+ cation into a

State Key Laboratory of Structural Chemistry, Fujian Institute of Research on the Structure of Matter, Chinese Academy of Sciences, Fuzhou, Fujian 350002, P. R. China. E-mail: gcguo@fjirsm.ac.cn, mswang@fjirsm.ac.cn

†Electronic supplementary information (ESI) available: Experimental details. Fig. S1–S5. See DOI: https://doi.org/10.1039/d3dt03080f

cyanide-bridged Mn^{II}–Fe^{III} inorganic framework as a photochromic organic functional motif,[42] we successfully obtained a photoactive semiconductor, $[\{Mn^{II-HS}(MQ)_2\}\{Fe^{III-LS}(CN)_6\}]Cl$ (**1** HS = high spin, LS = low spin), which showed a clear change of color and electrical properties with the generation of stable radicals after irradiation at RT.[43] Given the potential for photogenerated radicals to magnetically couple with paramagnetic centers and alter magnetic behavior,[44] we investigated the magnetic properties of compounds **1**. Our findings indicate that compound **1** exhibits a high degree of spin frustration, displaying antiferromagnetic coupling at RT and a spin canted antiferromagnetic glassy state at low temperatures before irradiation. After irradiation, compound **1** demonstrated photoinduced large magnetic change at room temperature and an unprecedented radical-quenched spin glass.

Single crystals of **1** were obtained according to our reported procedure and its crystal structure has been thoroughly defined.[43] So only the magnetic related structural information is discussed in detail here. The crystal structure of **1** features a 3-D supramolecular network, where 2-D inorganic layers are linked by π···π interactions between two adjacent MQ^+ ligands (Fig. 1). In the layer, each Fe^{III} atom coordinates to six cyano groups, while each Mn^{II} atom is ligated by two MQ^+ ligands and four cyano groups from four $[Fe(CN)_6]^{3-}$ units. Thus, two cyano groups of each $[Fe(CN)_6]^{3-}$ unit are mono-coordinated. This result agrees with the conclusion drawn from the IR spectra. The 2-D inorganic layer is similar to that in $RbMn^{II}[Fe^{III}(CN)_6]\cdot H_2O$ with a 3-D inorganic framework (Fig. 1).[45,46] However, the layers in **1** are stacked in parallel along the *c* axis without the displacement observed in the structure of $RbMn^{II}[Fe^{III}(CN)_6]\cdot H_2O$. The nearest metal atom from adjacent layers for each Fe^{III} atom is also the Fe^{III} atom, giving a Fe···Fe separation of ~13.50 Å. The shortest Fe···Mn, Fe···Fe and Mn···Mn distances in each layer are ~5.29 Å, 7.40 Å and 7.56 Å, respectively, which are comparable with those found in $RbMn^{II}[Fe^{III}(CN)_6]\cdot H_2O$.

As reported in our previous work'[43] compound **1** changed its color from brown (**1A**) to black (**1B**) upon irradiation with a Xe lamp (~50 mw cm^{-2}) at RT. Electron transfer from Cl/CN to MQ^+ concomitant with the generation of $MQ^{\bullet}$ radicals was proposed to interpret the coloration behavior. Other mechanisms including the photo-induced release of cyanide ligands similar to octacyanomolybdate[47] or electron transfer from Fe(III) to Mn(II) in $RbMn^{II}[Fe^{III}(CN)_6]\cdot H_2O$ were excluded because no obvious changes were observed in the PXRD pattern (Fig. S1†) or IR spectrum (Fig. S2†) after irradiation.

To explore the effect of photogenerated radicals on magnetic properties, the variable-temperature magnetic susceptibilities before and after irradiation were measured under a field of 1000 Oe in the temperature range of 2–300 K. As shown in Fig. 2a, the $\chi_M T$ value of **1A** at 300 K is 4.85 cm^3 K mol^{-1} per MnFe unit, which is slightly larger than the spin-only value of 4.75 cm^3 K mol^{-1} for one low-spin Fe^{III} (S_{Fe} = 1/2, assuming g_{Fe} = 2.00) and one high-spin Mn^{II} atom (S_{Mn} = 5/2, assuming g_{Mn} = 2.00). As the temperature is lowered, the $\chi_M T$ value decreases smoothly to a minimum of 4.36 cm^3 K mol^{-1} at 28.3 K, and then abruptly increases to reach a maximum of 11.31 cm^3 K mol^{-1} at about 4.95 K. Finally, the $\chi_M T$ value decreases again to 7.63 cm^3 K mol^{-1} at 2 K. This temperature-dependent behavior is typical for ferrimagnets as a result of an antiferromagnetic interaction.[45,46] The χ_M *vs.* *T* data between 50 and 300 K can be fitted to the Curie–Weiss law ($\chi_M = C/(T-\theta)$) with C = 4.89 cm^3 K mol^{-1} and θ = −5.25 K (Fig. S3†). The small negative Weiss constant indicates a weak antiferromagnetic interaction between Fe^{III} ($t_{2g}^5 e_g^0$) and Mn^{II} ($t_{2g}^3 e_g^2$) through the cyanide bridge, which is in accord with the theoretical inference based on the orbital-overlap principle.[22] The sharp peak of $\chi_M T$ at low temperature implies the long-range magnetic ordering below 5.0 K and the sharp decrease in $\chi_M T$ could possibly be attributed to the field saturation of the magnetic moment.

The variable-temperature alternating current (ac) susceptibility was recorded under zero dc to further confirm the magentic phase transition behavior. Apparent frequency-dependent peaks in the in-phase (χ') and out-of-phase (χ'') component are observed below 10 K. The peaks of the χ'' component are located at 3.18 K and 3.59 K for 10 and 1000 Hz, respectively, indicating the zero-field slow relaxation of magnetization. The shift of the peak temperature (T_p) in the plots of χ''–*T* was calculated to be 0.05 using the Mydosh parameter $\phi = (\Delta T_p/T_p)/(\Delta \log f)$, falling in the normal range for spin glass (ϕ < 0.08) (Fig. 3a). In addition, the temperature dependences of FCM (field-cooled magnetization) and ZFCM (zero-field-cooled magnetization) under an applied field of 5 Oe show an obvious

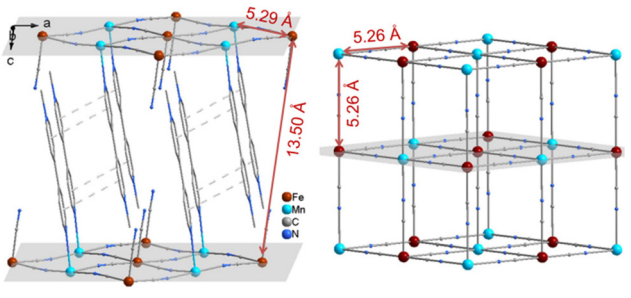

Fig. 1 Comparison of crystal structures between **1** (left, H atoms being omitted) and $RbMn^{II}[Fe^{III}(CN)_6]\cdot H_2O$ (right, only $Mn[Fe(CN)_6]^-$ is shown). The dashed lines depict π···π stacking interactions.

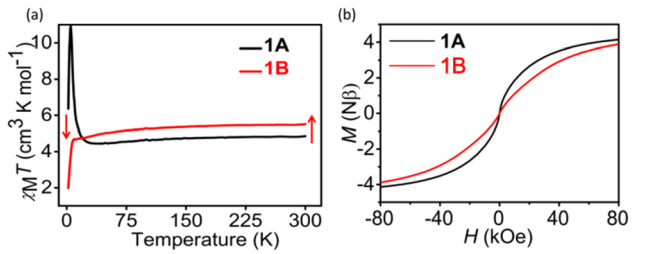

Fig. 2 (a) $\chi_M T$ *versus* *T* under *H* = 1000 Oe for **1A** and **1B**; (b) hysteresis loop of **1A** and **1B** measured at 2.0 K.

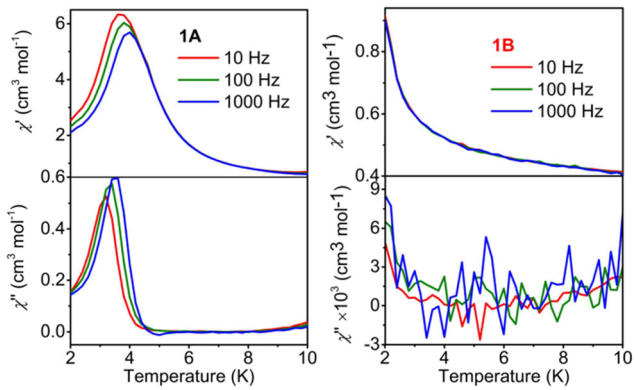

Fig. 3 χ' and χ'' *versus* T for **1A** (a) and **1B** (b) in 0 Oe dc and 2.5 Oe ac fields at various ac frequencies (10, 100, and 1000 Hz).

bifurcation below 5.0 K, further suggesting the blocking of the magnetization caused by spin glass behavior (Fig. S4†).

To check the magnetic hysteretic behavior of **1A** suggested by the irreversibility of the ZFC/FC curves below 10 K, the hysteresis loop at 2.0 K was measured. As can be seen, a hysteresis loop is observed with a coercive field (H_c) of 24 Oe and a remnant magnetization (M_r) of 0.014$N\beta$ (Fig. 2b and Fig. S5a†), further indicating the presence of spontaneous magnetization, consistent with the spin-glass antiferromagnetic behavior. Furthermore, the field dependence of the magnetization curve of **1A**, measured at 2 K, illustrates that the saturation of magnetization is completed at ~80 kOe (Fig. S5b†). At this point, the magnetization of ~4.15 $N\beta$ is very close to the expected value of 4 $N\beta$ for a Fe^{III-LS}–Mn^{II-HS} system with antiferromagnetic coupling ($M_s = g_{Mn}S_{Mn}N\beta - g_{Fe}S_{Fe}N\beta$, assuming $g_{Fe} = g_{Mn} = 2.0$). The $M(T)$ data measured at different applied fields in FC mode (Fig. 4a) exhibit a fine transition peak at about 4.5 K and a broad transition peak between 7.5 K and 12.5 K. Furthermore, the magnetization curves become flatter with increasing applied magnetizing fields, and the obvious transition peak almost disappears at 200 Oe (Fig. 4a) due to saturation of magnetization. All these results indicate that compound **1A** has a spin glass behavior below 5 K. These observations align with the alternating current (ac) data, which indicate spin glass ordering occurring at approximately 4.5 K (Fig. 3a).

Notably, the black color of the photoproduct is undesirable for the penetration of light to the interior of crystals.[48,49] So, we chose a YAG laser (4.1 mJ cm^{-2}) instead of the Xe lamp as a light source to obtain a colored sample for the magnetic study. The wavelength of the output light from the laser was monitored to the optimal photoresponsive wavelength of **1A**, *i.e.* 320 nm. As shown in Fig. 2a, after irradiation, the $\chi_M T$ value increased to 5.49 cm^3 K $mol^{-1}$and was 13.2% larger than that before irradiation, implying that new spins were generated after irradiation.

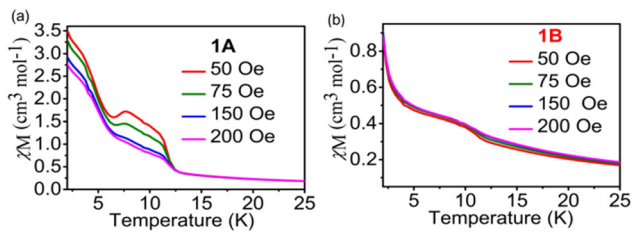

Fig. 4 Plots of χ_M *vs.* T at different fields for 1A (a) and 1B (b), respectively.

The photomagnetism of $RbMn^{II}[Fe^{III}(CN)_6]\cdot H_2O$ was caused by photo-induced Mn^{II}-to-Fe^{III} charge transfer.[45,46] As mentioned above, the photoinduced coloration of **1** was caused by Cl/CN → MQ^+ electron transfer, instead of Mn^{II}-to-Fe^{III} charge transfer, CN → Fe^{III} charge-transfer, d–d transition of Fe^{III}, and Mn^{II}-to-MQ^+ electron transfer. The increase of the $\chi_M T$ value for **1** upon irradiation can further rule out the occurrence of Mn^{II}-to-Fe^{III} charge transfer and Mn^{II}-to-MQ^+ electron transfer. The reason is that the $\chi_M T$ value would be largely reduced with the formation of diamagnetic Fe^{II-LS} ($t_{2g}^6e_g^0$), if the Mn^{II}-to-Fe^{III} charge transfer happens. In case of Mn^{II}-to-MQ^+ charge transfer, the $\chi_M T$ value would be almost retained for Mn^{III}–$MQ^{\bullet}$ ferromagnetic coupling or reduced for Mn^{III}–$MQ^{\bullet}$ antiferromagnetic coupling. All in all, the new spins are ascribed to the photogenerated radicals.

As shown in Fig. 2a, the $\chi_M T$ value for **1B** gradually decreased as the temperature was lowered, and went down sharply below 10 K to reach a minimum of 1.26 cm^3 K mol^{-1} at 2 K. The $\chi_M T$ values for **1B** are larger than those for **1A** in the range of 25–300 K but smaller than those for **1A** below 25 K. The χ_M *vs.* T data between 50 and 300 K can be fitted to the Curie–Weiss law with C = 5.56 cm^3 K mol^{-1} and θ = −5.65 K (Fig. S3b†). This θ value is smaller than that of **1A**, which means that the photogenerated radicals antiferromagnetically couple with metals. Koga *et al.* reported that Mn^{II} can antiferromagnetically couple with carbene radicals through the pyridyl bridge.[50] For **1B**, the metal–radical antiferromagnetical coupling should occur between Mn^{II} and $MQ^{\bullet}$. The M *vs.* H curve for **1B** becomes flat and is moved down compared with that of **1A**, but M does not increase linearly to H as occurs for a typical antiferromagnet (Fig. S5b†). So, the photoproduct of **1** is a ferrimagnet in nature.

The hysteresis loop at 2.0 K and variable-temperature alternating current (ac) susceptibility measurements were also performed for **1B** under zero dc. No hysteresis loop (Fig. S5a†), in-phase (χ') and out-of-phase (χ'') signals (Fig. 3b) as well as field-dependent transition peaks (Fig. 4b) can be found in the measured temperature range. All these results imply that the spin glass behavior was quenched by room temperature photo-induced coloration in **1B**. For **1A**, the slow magnetic relaxation and hysteresis loop are attributed to the spin glass behavior, which is most likely because of the disorder of the MQ ligands. However, the structural disorder should still exist in **1B** because no obvious structural change is observed after irradiation. The quenching of spin glass behavior for **1B** may be attributed to the generation of radicals, which have been reported to quench slow magnetic relaxation in molecule-based magnets.[51]

Ideally, one molecule of **1** can generate two radicals after irradiation. The $\chi_M T$ values at 300 K for **1A** and **1B** have a

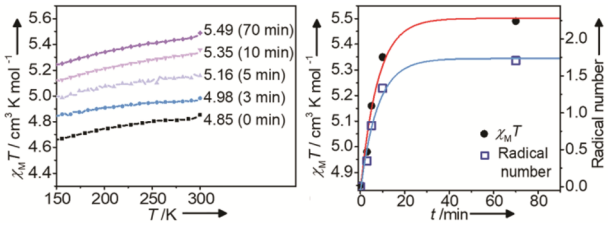

Fig. 5 χ_M *vs.* T with different irradiation times (left), and $\chi_M T$ and radical numbers (per molecule) *vs.* the irradiation time t at 300 K for **1** (right). A YAG laser (λ = 320 nm, 4.1 mJ cm^{-2}) was used as the light source. H = 1000 Oe. The red and pale blue curves denote the change tendency.

difference of 0.64 cm^3 K mol^{-1}, which theoretically corresponds to ~1.71 radicals per $[\{Mn^{II\text{–}HS}(MQ)_2\}\{Fe^{III\text{–}LS}(CN)_6\}]Cl$ molecule ($S_{radical}$ = 1/2, $g_{radical}$ = 2.0). We conducted a time-dependent magnetic susceptibility measurement at a field of 1000 Oe under YAG laser irradiation at 300 K for **1**. As shown in Fig. 5, with the increase in irradiation time, the curve of the radical number showed a trend similar to that of the $\chi_M T$ value. This reveals that the photomagnetism of **1** originates from the photogeneration of radicals, and the change in the $\chi_M T$ value is positively related to the number of radicals.

Conclusions

In summary, we successfully found a cyanide-bridged Mn^{II}–Fe^{III} compound with room-temperature photomagnetism, by incorporating the redox photoactive ligand MQ^+ into a 2-D cyanide-bridged inorganic framework. This photomagnet undergoes photoinduced electron transfer and yields stable radicals after irradiation at RT. The antiferromagnetic coupling between Mn^{II} and the photogenerated radical significantly changes the magnetism. Interestingly, this photomagnet shows spin glass behavior before irradiation, which can be turned off by room temperature light irradiation, showing the first example of radical-quenched spin glass in molecule based magnets. The new design strategy described in this work may help to obtain room temperature cyanide-bridged photomagnets with on/off slow magnetic relaxation behavior.

Author contributions

G.-C. Guo and M.-S. Wang conceived and supervised the project. L.-Z. Cai and X.-Q. Yu planned and implemented the synthesis and characterization of materials, and analysed data. L.-Z. Cai and M.-S. Wang wrote the manuscript. All authors discussed the results and commented on the manuscript.

Conflicts of interest

There are no conflicts to declare.

Acknowledgements

We gratefully acknowledge the financial support by the National Key Research and Development Program Ministry of Science and Technology (2021YFB3801604) and the National Natural Science Foundation (22371279, U21A20508, 22073102, 21827813, 21871264) of China.

References

1 W. Huang, X. Ma, O. Sato and D. Wu, *Chem. Soc. Rev.*, 2021, **50**, 6832.
2 O. Sato, T. Iyoda, A. Fujishima and K. Hashimoto, *Science*, 1996, **272**, 704.
3 S. Ohkoshi and H. Tokoro, *Acc. Chem. Res.*, 2012, **45**, 1749.
4 Y. Avila, P. Acevedo-Pena, L. Reguera and E. Reguera, *Coord. Chem. Rev.*, 2022, **453**, 214274.
5 D. Aguila, Y. Prado, E. S. Koumousi, C. Mathoniere and R. Clerac, *Chem. Soc. Rev.*, 2016, **45**, 203.
6 J. H. Wang, Z. Y. Li, M. Yamashita and X. H. Bu, *Coord. Chem. Rev.*, 2021, **428**, 213617.
7 T. Liu, Y.-J. Zhang, S. Kanegawa and O. Sato, *J. Am. Chem. Soc.*, 2010, **132**, 8250.
8 E. S. Koumousi, I.-R. Jeon, Q. Gao, P. Dechambenoit, D. N. Woodruff, P. Merzeau, L. Buisson, X. Jia, D. Li, F. Volatron, C. Mathonière and R. Clérac, *J. Am. Chem. Soc.*, 2014, **136**, 15461.
9 J.-X. Hu, L. Luo, X.-J. Lv, L. Liu, Q. Liu, Y.-K. Yang, C.-Y. Duan, Y. Luo and T. Liu, *Angew. Chem., Int. Ed.*, 2017, **56**, 7663.
10 L. Reguera, Y. Avila and E. Reguera, *Coord. Chem. Rev.*, 2021, **434**, 213764.
11 J.-D. Cafun, G. Champion, M.-A. Arrio, C. C. Moulin and A. Bleuzen, *J. Am. Chem. Soc.*, 2010, **132**, 11552.
12 T. Liu, H. Zheng, S. Kang, Y. Shiota, S. Hayami, M. Mito, O. Sato, K. Yoshizawa, S. Kanegawa and C. Duan, *Nat. Commun.*, 2013, **4**, 2826.
13 G. Li, T. Akitsu, O. Sato and Y. Einaga, *J. Am. Chem. Soc.*, 2003, **125**, 12396.
14 H. Tokoro, T. Matsuda, T. Nuida, Y. Moritomo, K. Ohoyama, E. D. L. Dangui, K. Boukheddaden and S.-i. Ohkoshi, *Chem. Mater.*, 2008, **20**, 423.
15 H. Svendsen, M. R. V. Jørgensen, J. Overgaard, Y.-S. Chen, G. Chastanet, J.-F. Létard, K. Kato, M. Takata and B. B. Iversen, *Inorg. Chem.*, 2011, **50**, 10974.
16 L. Zhao, Y.-S. Meng, Q. Liu, O. Sato, Q. Shi, K. Oshio and T. Liu, *Nat. Chem.*, 2021, **13**, 698.
17 S. Ohkoshi, K. Imoto, Y. Tsunobuchi, S. Takano and H. Tokoro, *Nat. Chem.*, 2011, **3**, 564.
18 S. Chorazy, T. Charytanowicz, D. Pinkowicz, J. H. Wang, K. Nakabayashi, S. Klimke, F. Renz, S. Ohkoshi and B. Sieklucka, *Angew. Chem., Int. Ed.*, 2020, **59**, 15741.
19 M. Reczynski, D. Pinkowicz, K. Nakabayashi, C. Nather, J. Stanek, M. Koziel, J. Kalinowska-Tluscik, B. Sieklucka,

S. I. Ohkoshi and B. Nowicka, *Angew. Chem., Int. Ed.*, 2021, **60**, 2330.
20 Q. Liu, J.-X. Hu, Y.-S. Meng, W.-J. Jiang, J.-L. Wang, W. Wen, Q. Wu, H.-L. Zhu, L. Zhao and T. Liu, *Angew. Chem. Int. Ed.*, 2021, **60**, 10537.
21 K.-P. Xie, Z.-Y. Ruan, B.-H. Lyu, X.-X. Chen, X.-W. Zhang, G.-Z. Huang, Y.-C. Chen, Z.-P. Ni and M.-L. Tong, *Angew. Chem., Int. Ed.*, 2021, **60**, 27144.
22 T. Mallah, S. Thiebaut, M. Verdaguer and P. Veillet, *Science*, 1993, **262**, 1554.
23 S. Koshihara, Y. Tokura, K. Takeda and T. Koda, *Phys. Rev. Lett.*, 1992, **68**, 1148.
24 S. Bonhommeau, G. Molnár, A. Galet, A. Zwick, J.-A. Real, J. J. McGarvey and A. Bousseksou, *Angew. Chem., Int. Ed.*, 2005, **44**, 4069.
25 H. Bouas-Laurent and H. Dürr, *Pure Appl. Chem.*, 2001, **73**, 639.
26 M. Estrader, J. S. Uber, L. A. Barrios, J. Garcia, P. LloydWilliams, O. Roubeau, S. J. Teat and G. Aromí, *Angew. Chem., Int. Ed.*, 2017, **56**, 15622.
27 M. M. Paquette, D. Plaul, A. Kurimoto, B. O. Patrick and N. L. Frank, *J. Am. Chem. Soc.*, 2018, **140**, 14990.
28 N. Kojima, M. Okubo, H. Shimizu and M. Enomoto, *Coord. Chem. Rev.*, 2007, **251**, 2665.
29 K. Matsuda, *Pure Appl. Chem.*, 2008, **80**, 555.
30 M. Morimoto, H. Miyasaka, M. Yamashita and M. Irie, *J. Am. Chem. Soc.*, 2009, **131**, 9823.
31 S. Venkataramani, U. Jana, M. Dommaschk, F. D. Sönnichsen, F. Tuczek and R. Herges, *Science*, 2011, **331**, 445.
32 K. Takahashi, Y. Hasegawa, R. Sakamoto, M. Nishikawa, S. Kume, E. Nishibori and H. Nishihara, *Inorg. Chem.*, 2012, **51**, 5188.
33 B. Rösner, M. Milek, A. Witt, B. Gobaut, P. Torelli, R. H. Fink and M. M. Khusniyarov, *Angew. Chem., Int. Ed.*, 2015, **54**, 12976.
34 K. S. Kumar and M. Ruben, *Coord. Chem. Rev.*, 2017, **346**, 176.
35 T. M. Bockman and J. K. Kochi, *J. Org. Chem.*, 1990, **55**, 4127.
36 G. Xu, G.-C. Guo, M.-S. Wang, Z.-J. Zhang, W.-T. Chen and J.-S. Huang, *Angew. Chem., Int. Ed.*, 2007, **46**, 3249.
37 Q.-K. Liu, J.-P. Ma and Y.-B. Dong, *J. Am. Chem. Soc.*, 2010, **132**, 7005.
38 J.-X. Hu, Q. Li, H.-L. Zhu, Z.-N. Gao, Q. Zhang, T. Liu and G.-M. Wang, *Nat. Commun.*, 2022, **13**, 2646.
39 B. Xia, Q. Gao, Z.-P. Hu, Q.-L. Wang, X.-W. Cao, W. Li, Y. Song and X.-H. Bu, *Research*, 2021, 549048.
40 Y.-J. Ma, J.-X. Hu, S.-D. Han, J. Pan, J.-H. Li and G.-M. Wang, *J. Am. Chem. Soc.*, 2020, **142**, 2682.
41 X.-Y. Lv, M.-S. Wang, C. Yang, G.-E. Wang, S.-H. Wang, R.-G. Lin and G.-C. Guo, *Inorg. Chem.*, 2012, **51**, 4015.
42 G.-C. Guo, Y.-G. Yao, K.-C. Wu, L. Wu and J.-S. Huang, *Prog. Chem.*, 2001, **13**(2), 151.
43 X.-Q. Yu, C. Sun, M.-S. Wang and G.-C. Guo, *Nat. Commun.*, 2020, **11**, 1179.
44 L.-Z. Cai, Q.-S. Chen, C.-J. Zhang, P.-X. Li, M.-S. Wang and G.-C. Guo, *J. Am. Chem. Soc.*, 2015, **137**(34), 10882.
45 S. Ohkoshi, H. Tokoro and K. Hashimoto, *Coord. Chem. Rev.*, 2005, **249**, 1830.
46 E. J. M. Vertelman, T. T. A. Lummen, A. Meetsma, M. W. Bouwkamp, G. Molnar, P. H. M. van Loosdrecht and P. J. van Koningsbruggen, *Chem. Mater.*, 2008, **20**, 1236.
47 X. Qi, S. Pillet, C. de Graaf, M. Magott, E.-E. Bendeif, P. Guionneau, M. RouziHres, V. Marvaud, O. Stefańczyk, D. Pinkowicz and C. MathoniHre, *Angew. Chem., Int. Ed.*, 2020, **59**, 3117.
48 J. Harada, R. Nakajima and K. Ogawa, *J. Am. Chem. Soc.*, 2008, **130**, 7085.
49 N. Leblanc, M. Allain, N. Mercier and L. Sanguinet, *Cryst. Growth Des.*, 2011, **11**, 2064.
50 N. Koga, Y. Ishimaru and H. Iwarnura, *Angew. Chem., Int. Ed. Engl.*, 1996, **35**, 755.
51 Q. Zhang, S.-D. Han, Q. Li, J.-X. Hu and G.-M. Wang, *Sci. China Mater.*, 2022, **65**(3), 788.